Vertical Motion in the Gulf Stream Near 68°W

SCOTT S. LINDSTROM AND D. RANDOLPH WATTS

University of Rhode Island, Graduate School of Oceanography, Narragansett Bay Campus, Narragansett, Rhode Island

(Manuscript received 6 October 1992, in final form 9 March 1994)

ABSTRACT

The authors compute and compare vertical motions from three different data sources within a 300-km square domain centered in the Gulf Stream near 38°N, 68°W, and show that vertical motions inferred from all three independent data sources and different analysis methods give similar results. The time derivatives of RAFOS float pressures on isopycnal surfaces are used to determine directly observed vertical motion w_{RAF}. Second, vertical motions are inferred from the heat equation using measured temperature changes and the backing and veering of currents observed by a stack of current meters to produce w_{CM}. Third, vertical motions are calculated from the quasigeostrophic vorticity equation using geostrophic streamfunctions from inverted echo sounder measurements to produce w_{IES}. w_{CM} agrees well with w_{RAF} from all floats that pass within 10 km of a current meter mooring. Daily fields of w_{IES} show very good coherence with time series of w_{CM} for periods longer than 16 d, but noise domination for periods shorter than 12 d. Typical magnitudes during strong "events" as estimated by all three data sources are on the order of 1–2 mm s^{-1} in regions near the center of the Gulf Stream. The characteristic spatial and temporal scales of upwelling or downwelling features are clearly defined from the horizontal maps and time series of w, and the location of these vertical motions relative to Gulf Stream mesoscale features is discerned.

1. Introduction

The vertical motion w of water parcels in the Gulf Stream is an important quantity to know for several reasons. Terms including vertical motion can be dominant in energy and vorticity analyses, and vertical motion is also a key component in cross-frontal circulations and nutrient cycling. Its small size relative to horizontal motions, however, has made it difficult to measure directly. Several methods have historically been used to estimate vertical motion in the ocean. For example, pressure records from isopycnal floats (Rossby et al. 1986) can be used to compute vertical motion directly along float tracks (Bower 1989; Bower and Rossby 1989). Bryden (1980), Hall (1986), and others have calculated vertical motion from stacked current meters (CM). This method, which is based on the quasigeostrophic heat equation, relates upward (downward) motion to veering (backing) currents with height and is similar to methods developed by Árnason (1942) and Panofsky (1944) for the atmosphere. Finally, Kim and Watts (1994) have shown that it is possible to determine a geostrophic streamfunction from objectively mapped fields of thermocline depth as determined from inverted echo sounder (IES) data. Because it is also possible to determine local tendencies of vorticity from the same data (Kim and Watts 1994), the quasigeostrophic vorticity equation [as in Holton (1979), for example] can be used to compute vertical stretching from the IES fields.

The main goals of this paper are to determine the degree of agreement between three different methods of computing vertical motion in the Gulf Stream and to characterize the structure of computed w fields relative to meanders. Previous studies of vertical motion have been limited to one data source in the Gulf Stream (e.g., Hall 1986, 1989; Osgood et al. 1987; Bower 1989; Bower and Rossby 1989; Blanton 1991) or to one-time snapshots elsewhere (e.g., Leach 1987). The dense dataset collected during the Synoptic Ocean Prediction (SYNOP) experiment and described in section 2 provides us with 1) observed vertical motions (from isopycnal RAFOS floats); 2) more than two years of point values of vertical motion inferred at 700 m from 12 CM moorings; and 3) more than two years of mapped vertical motions computed from IES data. The methods of computing vertical motion, described in section 3, are clearly distinct for each data source. In section 4, we compare the three different vertical motion estimates and find very good agreement, especially at long timescales. We combine all three data sources to describe both the temporal and spatial scales associated with vertical motion and the structural relationship between Gulf Stream meanders and vertical motion "events." In section 5, we relate the structure of vertical motion relative to Gulf Stream meanders to the conceptual model of Bower (1989) and Bower and Rossby

Corresponding author address: Dr. D. Randolph Watts, University of Rhode Island, Graduate School of Oceanography, Narragansett, RI 02882.

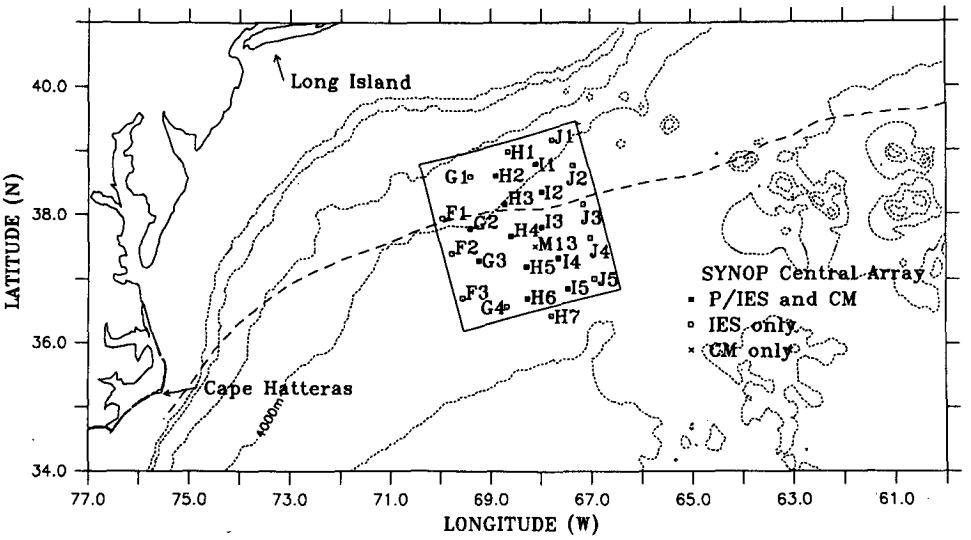

FIG. 1. Location of SYNOP central array in the Gulf Stream [mean location for 1975–1986 as inferred from satellite SST data (Gilman 1988) denoted by dashed line] northeast of Cape Hatteras. Bathymetry (contour interval of 1000 m) indicated. Instrumentation at each site as indicated in key.

(1989), namely, downwelling from crest to trough and upwelling from trough to crest, before concluding in section 6.

2. Data

All data were collected during 1988–1990 as part of the SYNOP experiment, an intensive multi-institutional study of the Gulf Stream between Cape Hatteras and 50°W. As part of the experiment, an array centered near 38°N, 68°W, where meanders commonly grow in amplitude [Gulf Stream meanders are discussed in more detail in Watts (1983)], and consisting of 24 IESs and 12 deep pressure sensors (Fields and Watts 1990, 1991) and 12 tall moorings with current meters at nominal depths of 400, 700, 1000, and 3500 m (Shay et al. 1994), was deployed from May 1988 through August 1990 (Fig. 1). We will refer to this region as the "Central Array," designating May 1988–May 1989 as "year 1" and August 1989–August 1990 as "year 2."[1] An additional component of the SYNOP experiment was the release of 75 isopycnal RAFOS floats (Anderson-Fontana and Rossby 1991) that were ballasted to stay near the 15°C isotherm. About 90% of these floats passed directly through the Central Array following paths that ranged from straight to s shaped to circular. We thus have a rich database with which to compute and compare vertical motions.

[1] Data from the intervening time, June–August 1989, were not yet ready when this analysis was started, and no RAFOS flybys occurred during this period.

3. Instruments and methods for determining vertical motion

a. *RAFOS floats*

The method for determining vertical motion from a ranging and fixing of sound (RAFOS) float w_{RAF} is straightforward. One of the variables recorded (three times daily) by the float is pressure. We used centered-in-time finite differencing to determine the pressure change (i.e., vertical motion). Because floats move *through* features, the vertical motion measured by the float, a 16-h average value, may differ from an instantaneous point value. This is most obviously the case if the float passes through an up/down couplet in 16 hours, in which case the average vertical motion may be near zero, although the values of upwelling or downwelling within the couplet (as sampled by a current meter mooring, perhaps) will not be. This bias error is discussed in detail in the appendix, in which we show that this method may underestimate several of the largest w events by as much as 30%. Errors introduced by the float not being perfectly isopycnal should be insignificant for the scales of motion we consider (H. T. Rossby 1992, personal communication).

b. *Current meters*

Bryden (1976, 1980) was among the first to use the backing (turning counterclockwise with decreasing depth) and veering (turning clockwise with decreasing depth) of current meters to infer vertical motion in the ocean. Following his notation, and that of Hall (1986), the temperature equation

$$\frac{\partial T}{\partial t} + u\frac{\partial T}{\partial x} + v\frac{\partial T}{\partial y} + w\frac{d\theta_0}{dz} = 0 \qquad (1)$$

can be transformed, using the thermal wind equation, to

$$w_{CM} = \frac{-\dfrac{\partial T}{\partial t} - \dfrac{\rho_0 f}{g\alpha_0}\left[v\dfrac{\partial u}{\partial z} - u\dfrac{\partial v}{\partial z}\right]}{\dfrac{d\theta_0}{dz}}$$

or

$$w_{CM} = \frac{-\dfrac{\partial T}{\partial t} - \dfrac{\rho_0 f}{g\alpha_0}R^2\dfrac{\partial \phi}{\partial z}}{\dfrac{d\theta_0}{dz}}. \qquad (2)$$

Here, R is the magnitude of the current velocity, ρ_0 is mean density (1035 kg m^{-3}), g is gravitational acceleration (9.8 m s^{-2}), f is the Coriolis parameter, α_0 is the effective thermal expansion coefficient

$$\equiv \frac{\partial \rho}{\partial T} + \frac{\partial \rho}{\partial S}\frac{\partial S}{\partial T} = 1.2 \times 10^{-1} \text{ kg m}^{-3}\text{ K}^{-1}$$

appropriate for the T–S relationship in midthermocline in the Gulf Stream (Hall 1985), $d\theta_0/dz$ is the mean stratification (0.02 K m^{-1}), ϕ is the angle of the current with respect to east, and u and v are the eastward and northward components of the flow. The constants used for this work are consistent with a Brunt–Väisälä period of about 20 min, which is approximately representative of the main thermocline in the Gulf Stream; however, we note later that w_{CM} could be biased slightly by this choice of constants.

For isentropic motions, vertical motion is proportional to the two terms in the numerator of (2). The first describes the motion of the isotherms themselves: for example, in the absence of horizontal motions, if the temperature at a current meter is increasing, isothermal surfaces, and the water parcels on them, must both be descending. The second term in the numerator is the heat advection in the presence of sloped isothermal surfaces, which is proportional to the cross-frontal component of velocity, as in (1), or equivalently to the turning of the current vector with height, $\partial\phi/\partial z$, as in (2).

The CM data used in this study have been smoothed. A 40-hour low-pass filter has been applied to the data to remove high-frequency signals (diurnal and semidiurnal tides, for example). In addition, the CM data have been adjusted to compensate for mooring motion. When strong currents surround a current meter mooring, it will tilt more than in an environment of weaker currents; therefore, the sensors do not always remain at the same level. The method of Hogg (1991) interpolates (or extrapolates) current meter measurements to constant horizons, in this case at 400, 700, and 1000 m below the sea surface. This mooring motion correction does not significantly affect the computed vertical motion. Furthermore, the corrected data yield vertical motions on one horizon throughout the domain. Therefore, in this study we used data corrected for mooring motion.

To compare w_{CM} with w_{RAF}, we selected those floats that passed within 10 km of a mooring on which all of the top three CMs were functioning. The 10-km cutoff was chosen as a compromise between increasing error (due to the highly sheared environment) as the distance increased from CM to float versus obtaining a useful number (23) of comparisons. The vertical motion w_{CM} was computed using (2), with the vertical derivatives ($\partial u/\partial z$ and $\partial v/\partial z$) approximated as centered finite differences using data at 400 and 1000 m. Current velocities (u and v) were averages of values at 400 and 1000 m. Temperature tendencies ($\partial T/\partial t$) were computed using a second-order centered-in-time finite-difference scheme with Δt = 12 hours. We originally used data here also at 400 and 1000 m; however, we discovered cases in which the main thermocline moved significantly, as measured at 700 m, without greatly changing the temperature measurements at 400 and 1000 m, because these depths were at the time above and below the main thermocline, respectively. To account accurately for vertical motion associated with temperature changes it was necessary to use the temperature at 700 m to compute $\partial T/\partial t$. Using the 700-m currents, however, added no new information to the w_{CM} calculation. The total vertical motion computed can be considered as a representative value about halfway between 400 and 1000 m. We have used the formula including $v\partial u/\partial z - u\partial v/\partial z$ because it gives more smoothly varying results than the formula including $R^2\partial\phi/\partial z$. The R^2 term introduced spikes into the results when the current speed profile was not linear.

Finally, we carefully scrutinized the CM data records to make certain that no rapid strong fluctuations in current speed or direction were present when float comparisons were made. We wished especially to avoid using CM data during time periods that contained submesoscale coherent vortices (SCVs), which Bane et al. (1989) have observed in the Gulf Stream to cause sporadic rotations of up to 360° in the current vector as well as a temperature perturbation at one CM on a mooring. The presence of an SCV obviously would adversely impact this primarily quasigeostrophic study. No evidence of such fluctuations was found in any 5-day interval of CM data centered on the 23 closest-passing float cases studied here.

c. *Inverted echo sounders*

Inverted echo sounders sit on the ocean floor and acoustically monitor the depth of the main thermocline, as indicated by the 12° isotherm depth (z_{12})

(Watts and Rossby 1977). To compute vertical motion from IES data, we used objectively mapped IES data (Tracey and Watts 1991) to determine a streamfunction and therefore a relative vorticity field, both valid at 400 m relative to 3500 m, as in Kim and Watts (1993). (Note that this streamfunction is not the same as a streamfunction on the sloping 12° isotherm surface.) As with CM data, all IES data are 40-h low-pass filtered to remove high-frequency signals. This smoothing is done before the objective mapping. The IES fields are objectively mapped daily for 26 months, yielding estimates not only of streamfunction and relative vorticity but of the time tendencies of both. If the motion is assumed to be quasigeostrophic, then the vorticity equation as in, for example, Holton (1979)

$$\frac{\partial \zeta_g}{\partial t} = -\mathbf{V}_g \cdot \nabla(\zeta_g + f) + f_0 \frac{\partial w}{\partial z}, \qquad (3)$$

can be used to estimate vertical stretching. Vertical motion in the Gulf Stream has primarily a first baroclinic mode structure (Hall 1986; Rossby 1987). The maximum vertical motion occurs below the main thermocline (Gill 1982, Fig. 6.14); even for very shallow main thermoclines (i.e., z_{12} around 200 m—much shallower than for any case we consider here), the methods used in Pickart and Watts (1990) show that the maximum in vertical motion is below 500 m. Vertical motion in the upper ocean at depth z can therefore be approximated as

$$w_{\mathrm{IES}} = \frac{z}{f_0}\left[\frac{\partial \zeta_g}{\partial t} + \mathbf{V}_g \cdot \nabla(\zeta_g + f)\right], \qquad (4)$$

using data at 400 m. Note that although both (2) and (4) are derived assuming quasigeostrophic balance, the assumption is applied to different equations, namely, to the heat equation for (2) and to the vorticity equation for (4). The validity of using the quasigeostrophic assumption in the Gulf Stream is considered in section 5c.

We have used (4) to compute vertical motions instead of the quasigeostrophic ω equation as used by Leach (1987), Tintoré et al. (1991), and Pollard and Regier (1992) because it is more suited to our data. In the other studies, roughly synoptic CTD data were available to provide data at different levels as is necessary for Q-vector computations. We have a streamfunction map at just one level, but at a sequence of times, making (4) a more natural way to compute vertical motion. The definition of the geostrophic streamfunction is as in Kim and Watts (1993); namely,

$$\mathbf{V}_g = \frac{g^*}{f_0}\,\mathbf{k} \times \nabla z_{12}, \qquad (5)$$

where we have used for $g^*(\equiv g\Delta\rho/\rho)$ a value that is a weak function of z_{12}, the depth of the 12° isotherm.[2] The geostrophic current thus computed, from which $\partial w/\partial z$ is computed, is valid at 400 m, referenced to 3500 m, where no motion is assumed.

To generate the field of vertical motion, we estimated the time tendency $\partial \zeta_g/\partial t|_{t=t_0}$ using a centered finite difference

$$\frac{\zeta_g(t_0 + \Delta t) - \zeta_g(t_0 - \Delta t)}{2\Delta t},$$

with Δt = 24 hours. Vorticity advection (relative plus planetary) was computed at time t_0 with horizontal derivatives computed using second-order centered finite differencing. We have smoothed the IES streamfunction fields with three applications of a Shapiro second-order filter (Shapiro 1970) to reduce the amount of noise in the highly differentiated vertical motion field. Such smoothing reduces values of extrema in the resultant vertical motion field without changing their location. The filter wavelength cutoff is −6 dB at 133 km; features with length scales = $k^{-1} > 37$ km are passed with greater than 80% amplitude. The gridded values of w_{IES} were interpolated to each CM location so that direct comparisons could be made between w_{CM} and w_{IES}. These comparisons can occur at sites that may not be in the best IES mapping region; therefore, the IES to RAFOS comparison may not be as good as the CM to RAFOS comparison. Indeed, we do not include any w_{IES} values at CM location I5 in this study. The location of this site at the southern edge of the IES array implies that vorticity and vorticity advection cannot be properly specified at I5; in fact, w_{IES} is of the wrong sign for each of the comparisons to w_{RAF} at I5. Thus, there are 23 w_{CM} versus w_{RAF} comparisons in this paper but only 13 w_{IES} versus w_{RAF}.

4. Results

a. Statistics and scales of vertical motion

Table 1 shows the general statistics of vertical motion in the Central Array: the means, standard deviations, maxima, minima, and the number of observations for the two-year period for each data source. All data sources within the Central Array indicate mean downwelling. The larger mean value of w_{RAF} may reflect a sampling bias: floats remained mostly within the strongly baroclinic structure of the central Gulf Stream when traversing the Central Array, whereas CM and IES measured vertical motions throughout the region spanning also the slope and Sargasso waters where large-scale vertical motions are smaller. Note that w_{RAF}

[2] Note that the CM data are used in the computation of g^* (Kim and Watts 1993). Strictly speaking, then, w_{CM} and w_{IES} are not independent, although of course CM data and IES data are. The fit used to compute the best g^* is optimized in an rms sense for a few CM sites. From that data we derive an entire field whose day-to-day variations come from data that is independent of CM and RAFOS data.

downwelling averaged over all tracks, including those that escaped the Gulf Stream, is an order of magnitude smaller than within the Central Array. We are examining a segment of the Gulf Stream that, for these 26 months at least, was experiencing mean downwelling.

How representative are the mean vertical motions in Table 1? Although it is difficult to quantify the statistical significance of the means (i.e., we cannot claim with certainty that our mean is representative of the true long-term mean in this region), we note that the mean IES data (Fig. 2) suggests IES are preferentially sampling a crest to trough portion of the Gulf Stream in the Central Array. Bower (1989) shows downwelling occurring on RAFOS float crest to trough segments. Furthermore, we note that Lee (1993), using satellite infrared imagery, detects a trough in the mean path in the area of the Central Array for 6 out of 8 years. Taken together, these facts do suggest some significance to the mean values in Table 1.

Before we make detailed comparisons of the measurement methods, it is useful to note the spatial and temporal scales of upwelling and downwelling motions. (The veracity of the maps and time series is justified by the comparisons to be made shortly.) The vertical motions computed from mapped IES data are horizontally and temporally coherent and smoothly varying. As an example, consider Fig. 3, which presents the objective mapping of the z_{12} topography together with w_{IES} (contoured with an interval of 0.2 mm s^{-1}) as computed from (4) every two days from 9 to 15 May 1990. A meander trough propagates through the Central Array and strengthens; vertical motion is diagnosed where conceptual models (cf. Bower and Rossby 1989) place it. Downwelling is diagnosed between crest and trough, upwelling between trough and crest. The strongest vertical motion (±2 mm s^{-1}) occurs in the middle of the Gulf Stream, roughly halfway between troughs and crests. Minimal vertical motion is diagnosed in slope or Sargasso waters. Furthermore, as the meander trough propagates, so too do the diagnosed vertical motion patterns.

We now present several figures that give evidence that the vertical motion determined from all three data sources is usually consistent. Figure 4 shows two time series of w_{CM} and w_{IES} at two unrelated sites and times, G2 and I1, that are representative of several strong

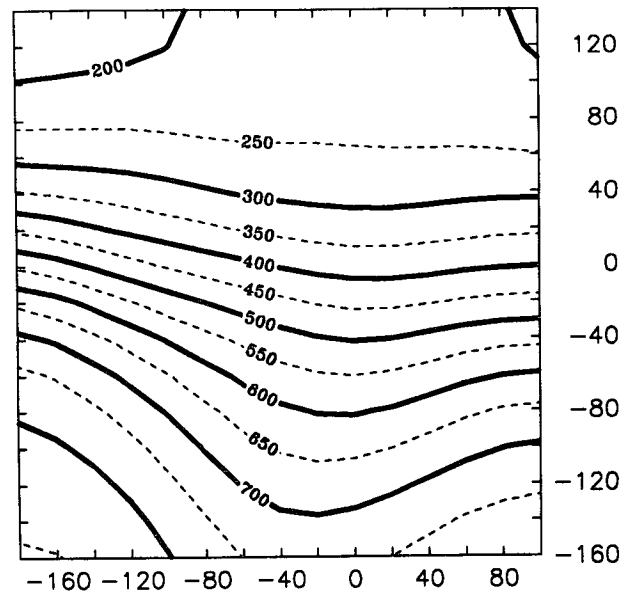

FIG. 2. Mean z_{12} topography (contoured every 50 m, bold lines every 100 m, dashed every 50 m) for the period 15 June 1988–7 August 1990 within boxed region of Fig. 1; x and y axis labels are kilometers.

events of upwelling and downwelling at all the CM sites. There are clear similarities between w_{CM} and w_{IES}: both show events of upwelling and downwelling that develop and pass coherently with some high-frequency noise, extrema are approximately collocated, signal strength is similar in the two lines, and the episodic nature is obvious. We have made a similar comparison for both years at each CM mooring location that had all three upper CMs functioning and that was surrounded by functioning IESs. The similarity evident in Fig. 4 characterizes all such sites: large vertical motion in one data source usually has a corresponding extremum in the other; however, some counterexamples will be shown. Examples of the w records along the H line of current meters (H3, H5, and H6 from year 1 and H4 and H6 from year 2) are shown in Figs. 5a–e, where the characteristics highlighted in Fig. 4 are again evident. Note that in each time series, a large peak in vertical motion in one method generally has a

TABLE 1. Vertical motion statistics. Mean, maximum, and minimum vertical motion (in mm s^{-1}) with standard deviation and number of observations for CM, IES (not all independent), RAFOS floats in the Central Array only, and for all RAFOS floats.

Source	Mean	Std dev	Maximum	Minimum	Number of observations
Current meters	−0.015	0.347	3.676	−2.297	25 419
Mapped IES	−0.027	0.440	4.006	−3.794	188 640
RAFOS in Central Array	−0.048	0.617	2.10	−2.66	947
All RAFOS	−0.006	0.532	3.30	−3.34	5939

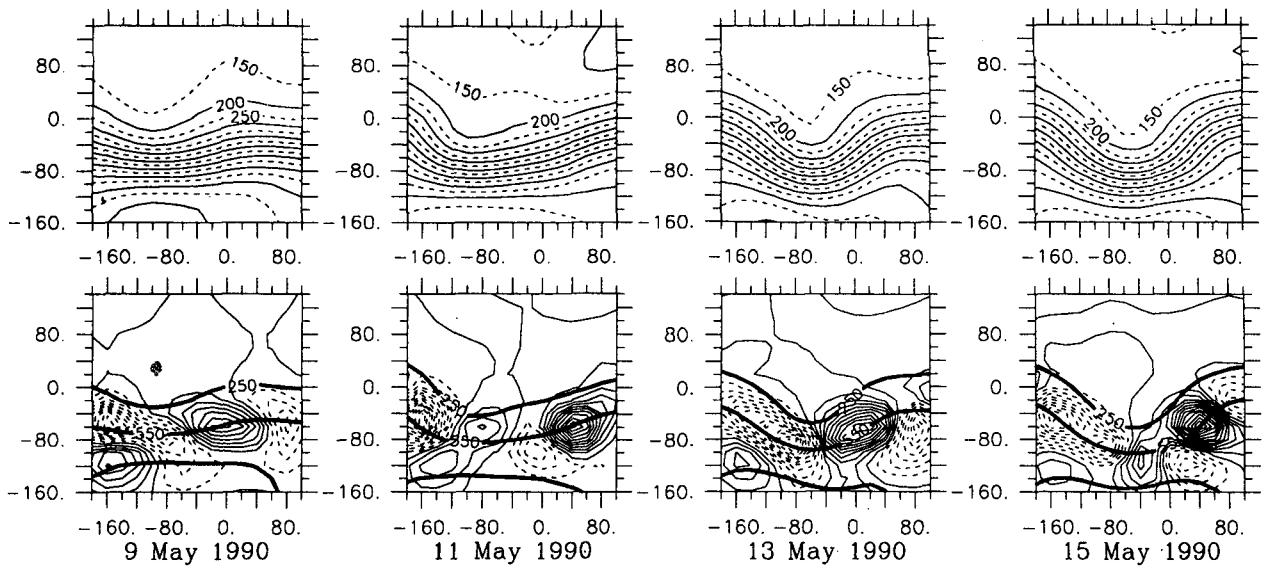

FIG. 3. Mapped z_{12} topography (top, contour interval 50 m) and vertical motion w_{IES} (bottom, contour interval 0.25 mm s^{-1}, negative values dashed) overlying z_{12} topography (bold lines, contour interval 300 m) every other day from 9 to 15 May 1990 in Central Array; x and y axis labels are kilometers.

corresponding peak in the other, although some time series (e.g., Fig. 5b) are better than others. There is intertime series variability as well. Compare, for instance the first half of Fig. 5d, which shows little coherence, with the second half, which shows considerably more. Despite occasional short period discrepancies between methods, we will show below that, overall, the time series of w_{CM} and w_{IES} are coherent at periods longer than 12 days.

b. A case study

Now consider Fig. 6, which shows the IES streamfunction field and the quasigeostrophic w_{IES} when RAFOS float 201 (whose entire 5-day track through the Central Array is indicated) passes within 10 km of current meter I1 (Note that Fig. 4 presented the I1 time series data with a peak in upwelling centered on this same event.) Surrounding site I1 is a strong upwelling

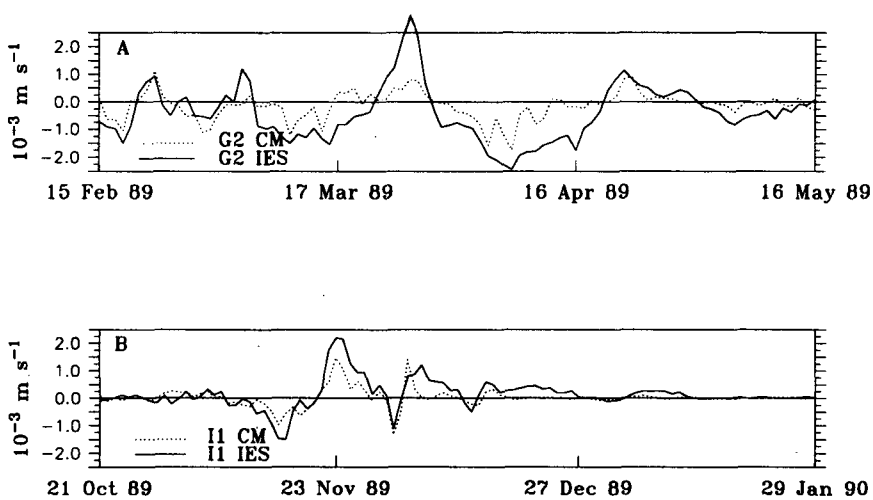

FIG. 4. Time series of vertical motion for (a) CM G2 and (b) CM I1 with dates as indicated on the x axis. Vertical motion from CM data (w_{CM}) using Eq. (2) is indicated with dotted line; that from IES data (w_{IES}) and Eq. (4) is indicated with the solid line.

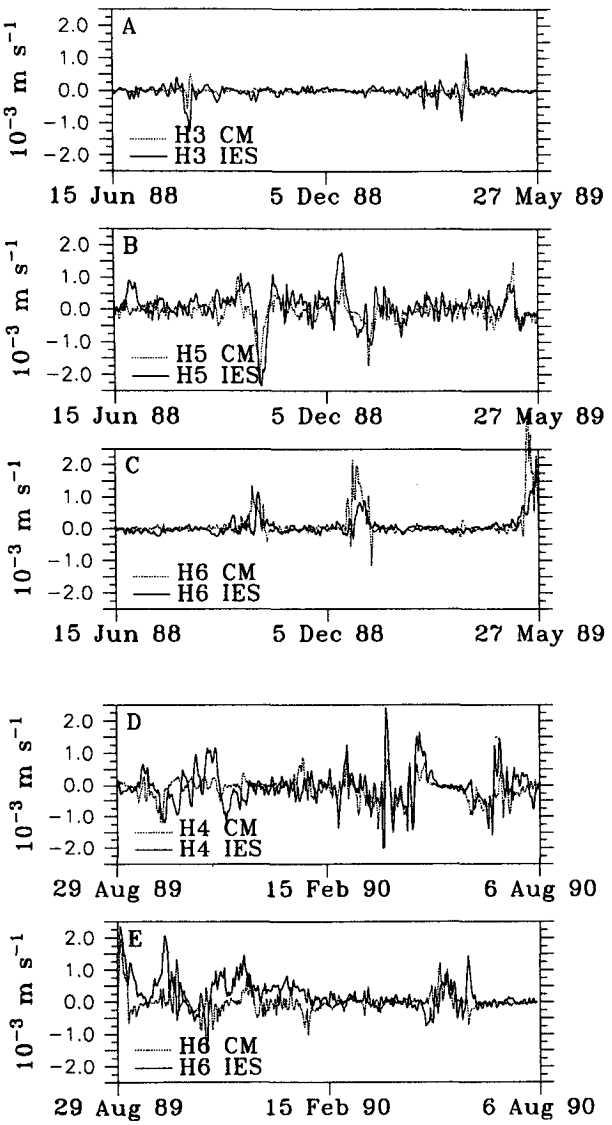

FIG. 5. As in Fig. 4 except for (a) CM H3, year 1; (b) CM H5, year 1; (c) CM H6, year 1; (d) CM H4, year 2; and (e) CM H6, year 2.

region in a trough to crest segment of path; it is traversed by the float that confirms the upwelling in a manner consistent with the work of Bower (1989). At the closest approach to CM I1, the float's upward velocity is 0.97 mm s^{-1}. This agrees qualitatively with the value from the quasigeostrophic vorticity equation (4) (w_{IES} = 1.66 mm s^{-1}) and with the value from the CM method (2) (w_{CM} = 1.51 mm s^{-1}); that is, all three methods show large upward velocity.

Dynamically, the IES method diagnoses vertical motion because of the sharp propagating trough just upstream of CM I1. Indeed, at the time float 201 passes CM I1, the baroclinic streamfunction suggests that, in one day, absolute vorticity advection will cause the vorticity to increase by 30% of f, the planetary vorticity. However, the observed vorticity increase, that is, $\partial\zeta_g/\partial t$, is only 5% of f. The apparent imbalance between local and advective changes in vorticity is reconciled by divergence, which eliminates most of the cyclonic vorticity advected over site I1. This divergence is accompanied by vigorous upwelling. This quasigeostrophic mechanism is associated with downwelling downstream of crests and upwelling downstream of troughs.

The dynamics of the observed vertical motion could also be expressed in terms of potential vorticity as in Pollard and Regier (1992). For example, as water columns above the main thermocline move into an environment of increasingly anticyclonic vorticity (by moving toward a crest, for example), the columns will acquire anticyclonic spin; that is, their vorticity will decrease. To conserve potential vorticity, the water column must shrink, which is accomplished by upwelling and the ascent of water within the main thermocline.

Current meter data and (2) also indicate upward vertical motion when the float passes CM site I1. In Fig. 7 we show time series of terms in (2) that contribute to w_{CM} for the 5 days bracketing this float passage. The advective term, shown in panels a, b, and c, is associated with consistent veering of the currents. When float 201 passes CM I1, 400-m currents are

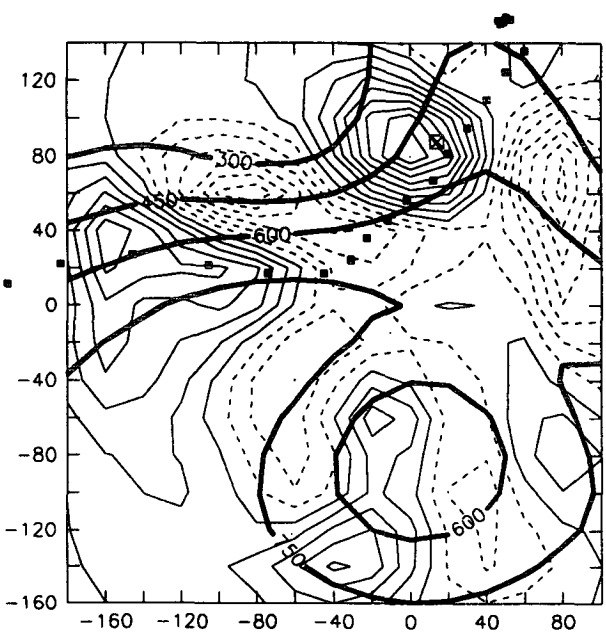

FIG. 6. Mapped thermocline topography, that is, z_{12}, (bold, contour interval 150 m) as measured by IES at 0800 UTC 23 November 1989 overlaid by w_{IES} computed from (4) (contour interval 0.25 mm s^{-1}, negative values dashed). Also indicated are the track of RAFOS float 201 [small boxed x's at 8-h intervals on the (approximately) 14.5° temperature surface], and the location of CM I1 (large boxed x), to which float 201 was closest at the time of this map.

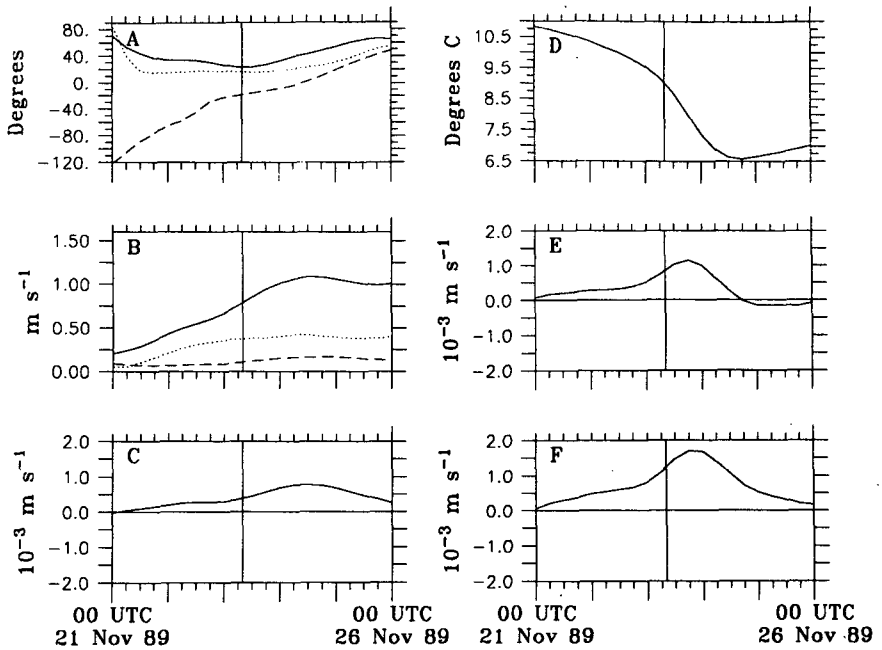

FIG. 7. Time series of terms contributing to w_{CM} in Eq. (2) at CM I1. Data are every 6 h from 0000 UTC 21 November 1989 through 0000 UTC 26 November 1989. The date/time when float 201 passes by CM I1, 0800 UTC 23 November 1989, is indicated by the vertical lines. (a) Direction (degrees from true north) toward which water is flowing. (b) Current speed (m s^{-1}). For both (a) and (b), solid lines are for 400 m, dotted lines for 700 m, and dashed lines for 1000 m. (c) Vertical motion (mm s^{-1}) due to advection. (d) Temperature (°C) and (e) associated vertical motion (mm s^{-1}) as measured at 700 m. (f) Total vertical motion (mm s^{-1}) – the sum of (c) and (e).

flowing to the northeast at about 0.8 m s^{-1}; 1000-m currents are flowing toward the north-northwest at 0.1 m s^{-1}. The thermal wind in this case points northeast: isothermal surfaces slope up to the northwest. The mean current therefore has a substantial cross-frontal component manifest as a significant "uphill" component along the sloping isothermal surface. Also when float 201 passes CM I1, the temperature at the CM is cooling as seen in panel d, reflecting upward vertical motion. Vertical motion associated with rising/sinking isothermal surfaces (panel e) is also upward, and the sum vertical motion (panel f) is large. Case studies for all 23 events in Table 2 can be found in Lindstrom and Watts (1993).

c. *Comparisons between all three methods*

Table 2 presents comparisons of vertical motion for all 23 cases in which a float passed within 10 km of a CM mooring with working instrumentation at 400, 700, and 1000 m. At such times, we can compare w_{RAF} with w_{CM} and w_{IES}. Figure 8a is a scatterplot of RAFOS vertical motions versus CM vertical motions, with data taken from Table 2. A linear relationship is clearly evident with correlation $r^2 = 0.82$. (Confidence level is much greater than 99%.) Indeed, this plot serves to underscore a point made by Hall (1986): in the Gulf Stream, meaningful conclusions can be drawn using quasigeostrophic diagnostics on observational data. That the slope of the line in Fig. 8a is greater than unity could arise from our values of α_0 or $d\theta_0/dz$ in (2) or from w_{RAF} being biased low, as discussed in section 3. However, the plot underscores the excellent agreement between w_{RAF} and w_{CM}.

The comparison in Fig. 8b between w_{RAF} and w_{IES} for the same cases (excluding site I5 as explained at the end of section 3) shows more scatter. Nevertheless, after eliminating the outlier that is discussed below, the correlation is $r^2 = 0.51$, which is significant at a confidence level of greater than 90%. The slope of the regression line is unity. To understand the causes of errors in this scatterplot, we have closely investigated the fields associated with the outlier in Fig. 8b. It has easily identifiable errors as discussed below.

The point in the lower right quadrant of Fig. 8b is from the case when RAFOS float 194 passed by CM I4 at 0000 UTC 16 November 1989. Both CM and float vertical velocities are upward; however, IES vertical motion is downward. This may be caused for two reasons. The first reason is related to poor IES data at site I4 during winter of year 2, when this IES suffered from many bad data returns, necessitating frequent interpolations to compute thermocline depth at that site (Fields and Watts 1991). Such data degradation would

TABLE 2. Vertical motion triple comparisons. Vertical motions from RAFOS float, CM, and IES data (w_{RAF}, w_{CM}, and w_{IES}, respectively), with units of millimeters per second for date/time (Z ≡ h UTC) shown and for RAFOS float and CM indicated. Depth of the RAFOS float at the comparison time (in meters) is also shown.

Float	CM	Date/time	w_{RAF}	w_{CM}	w_{IES}	Depth
RAF123	H4	4Jul88/00Z	−0.58	−0.98	−1.42	550.3
RAF129	I4	23Sep88/08Z	0.19	0.53	0.04	710.7
RAF129	I4	23Sep88/16Z	0.72	0.48	0.05	706.4
RAF136	I4	8Dec88/16Z	0.81	0.43	0.17	668.4
RAF141	I4	2Nov88/16Z	−0.87	−0.94	−0.43	603.0
RAF175	I4	20Jan89/16Z	−0.56	−0.05	−0.63	363.7
RAF176	I5	7Feb89/00Z	−0.04	0.02	—	761.5
RAF176	I5	7Feb89/08Z	−0.05	0.03	—	763.0
RAF176	I5	7Feb89/16Z	0.04	0.02	—	764.5
RAF176	I5	8Feb89/00Z	−0.03	−0.05	—	760.7
RAF194	I5	15Nov89/00Z	0.71	0.23	—	662.2
RAF194	I4	16Nov89/00Z	0.86	1.20	−1.06	584.3
RAF199	I5	23Nov89/00Z	0.24	0.23	—	593.2
RAF199	I5	28Nov89/16Z	−0.13	0.04	—	627.4
RAF201	I1	23Nov89/08Z	0.97	1.51	1.66	560.4
RAF207	I2	4Sep89/08Z	−0.25	−0.06	−0.24	164.0
RAF209	I5	13Sep89/08Z	−1.53	−2.14	—	629.2
RAF210	H4	6Oct89/08Z	−0.02	−0.19	−0.84	642.4
RAF210	I5	21Oct89/00Z	0.36	1.07	—	557.4
RAF211	M13	8Oct89/00Z	−0.44	−0.68	−0.78	658.9
RAF216	I1	26Nov89/00Z	−0.02	0.14	0.86	576.2
RAF221	I2	6Jan90/08Z	0.18	0.21	0.45	482.9
RAF224	H4	20Jan90/08Z	−0.18	−0.10	−0.30	496.7

of course have a negative impact on the computed streamfunction field and all quasigeostrophic calculations near I4 for winter 1989/90 data.

It is far more likely that the errors were introduced into w_{IES} because at this time significant currents were observed at deep levels. IES measurements infer the baroclinic component of the flow only; if there is significant barotropic flow, the currents (and therefore the vorticities and advections) inferred from the IES data may be in error. Figure 9 presents the thermocline topography and w_{IES} for this time, as well as the track of float 194 as it traversed the central array. We have also plotted the deep currents at the CM sites. Note the unusually strong flow at 3500 m at I4. In this area, strong upward motion associated with onshore cyclonically curved barotropic flow overwhelms the downward vertical motion associated with the baroclinic flow. In fact, this event is associated with the strongest deep currents for the w_{IES} cases present in Table 2: ($|\vec{v}_{3500}| = 0.19$ m s^{-1}, which is a value nearly two standard deviations above the mean speed at I4 in year 2.)

d. Coherence between w_{CM} and w_{IES}

All time series estimates of w_{CM} and w_{IES} (e.g., Figs. 4 and 5) show smoothly varying signals with varying degrees of high-frequency noise superimposed. We spectrally decomposed each pair of records and computed their statistical coherence at all sites along the central mooring H line whose time series were shown in Fig. 5. These coherence results were averaged for the whole line and are shown in Fig. 10. The average coherence between the two independent estimates of vertical motion is greater than 0.5 (far above the 99% confidence level) throughout all periods longer than 16 days. At periods shorter than 12 days, the coherence is insignificant. This confirms the visual impression from Fig. 5 that the large amplitude, low-frequency variations of w from both CM and IES techniques are very consistent, while the smaller amplitude, high-frequency variations are noise dominated.

Given these statistical coherences, how well can we use Eqs. (2) and (4) to infer vertical motion using data from the CM and IES arrays that were designed for mesoscale sampling? Both techniques involve temporal and spatial differentiation of measured quantities, an analysis which accentuates measurement and sampling errors. The errors in w_{CM} from (2) are dominated by submesoscale features whose signal is incoherent between our different moored u, v, T sensors rather than by measurement error. Errors in w_{IES} from (4) are dominated by instrument/analysis error in the streamfunction fields: the objective mapping and measurement techniques filter out submesoscale features, including some that may be sampled at individual CM moorings. Nevertheless, with either technique, the major mesoscale features in w are clear. The coherence between w_{IES} and w_{CM} shown in Fig. 10 and the particularly good agreement between w_{RAF} and w_{CM} illustrated in Table 2 and Fig. 8a; that is, agreements between three different techniques for measuring w, show that the $w_{CM}(t)$ and $w_{IES}(x, y, t)$ fields do characterize mesoscale vertical motions in the Gulf Stream.

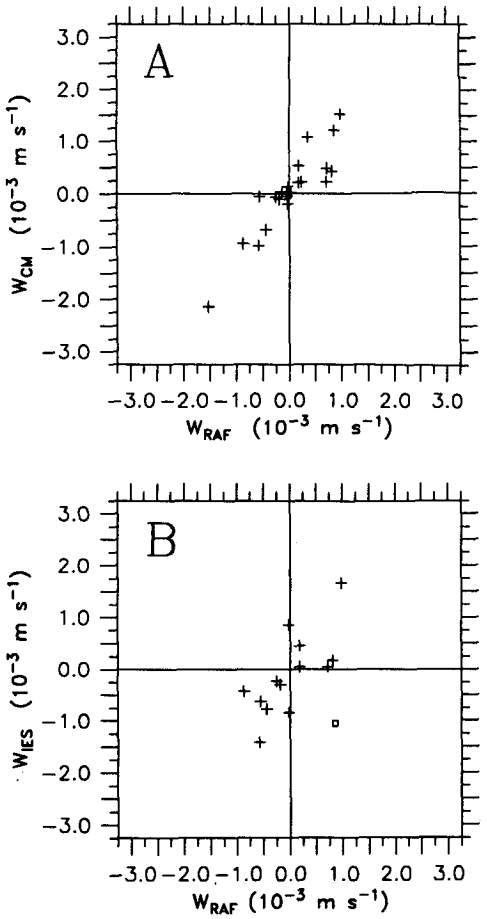

FIG. 8. (a) Scatterplot of w_{RAF} vs w_{CM} as listed in Table 2. (b) Scatterplot of w_{RAF} vs w_{IES} as listed in Table 2. Open square in (b) is discussed further in the text.

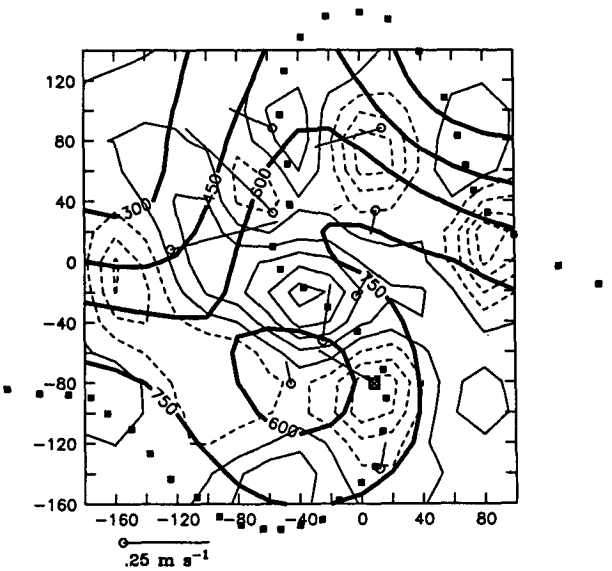

FIG. 9. As in Fig. 6 but for RAFOS float 194 passing CM I4 at 0000 UTC 16 November 1989. Deep currents are plotted at CM sites as line segments, with a scale indicated at lower left.

5. Structure of vertical motion in the Gulf Stream

Using all of the above observations, we can create a picture of the structure of Gulf Stream meanders. Progressing downstream from a trough to a crest, currents veer with height: the current toward the northeast near the surface turns more toward the north (i.e., onshore, across the Gulf Stream front) with increasing depth. Such a current structure is consistent with our observed vertical motion pattern (upward) and with the notion that Sargasso Sea water is entrained into the stream between trough and crest (Bower and Rossby 1989). Progressing downstream from a crest to a trough, backing of currents with height occurs. Surface flow toward, for example, the southeast will turn more toward the south (offshore, across the Gulf Stream front) with increasing depth, consistent with the entrainment of slope water into the stream and downward motion.

Strong vertical motions are diagnosed as eastward-moving meanders slow or become nonpropagating. Note that these observations directly contradict the simple kinematic model of Bower (1991), which predicts no vertical motion for a stationary meander. Figure 11 shows a representative nonpropagating meander. We show gridded z_{12} data, as measured from IES, on 19 May and 27 May 1990, when a deep meander trough did not propagate; superimposed upon these are the fields of w_{IES}. Strong vertical motion is diagnosed on both days, and it remains locked in place with the structure of the meander throughout this period. Current meter data (not shown) also diagnose large vertical motion, with downwelling at CM G3 [located at (−125, −48)] and upwelling at CM I4 [(6, −80)]. Large values of divergence for a stationary wave,

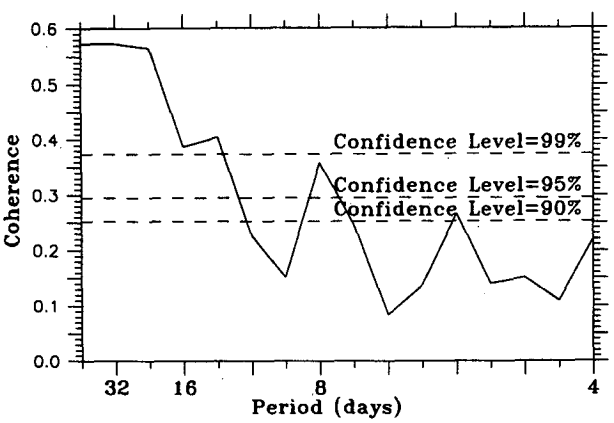

FIG. 10. Coherence as a function of frequency for w_{IES} and w_{CM} for CM sites on the H line. Confidence levels as indicated.

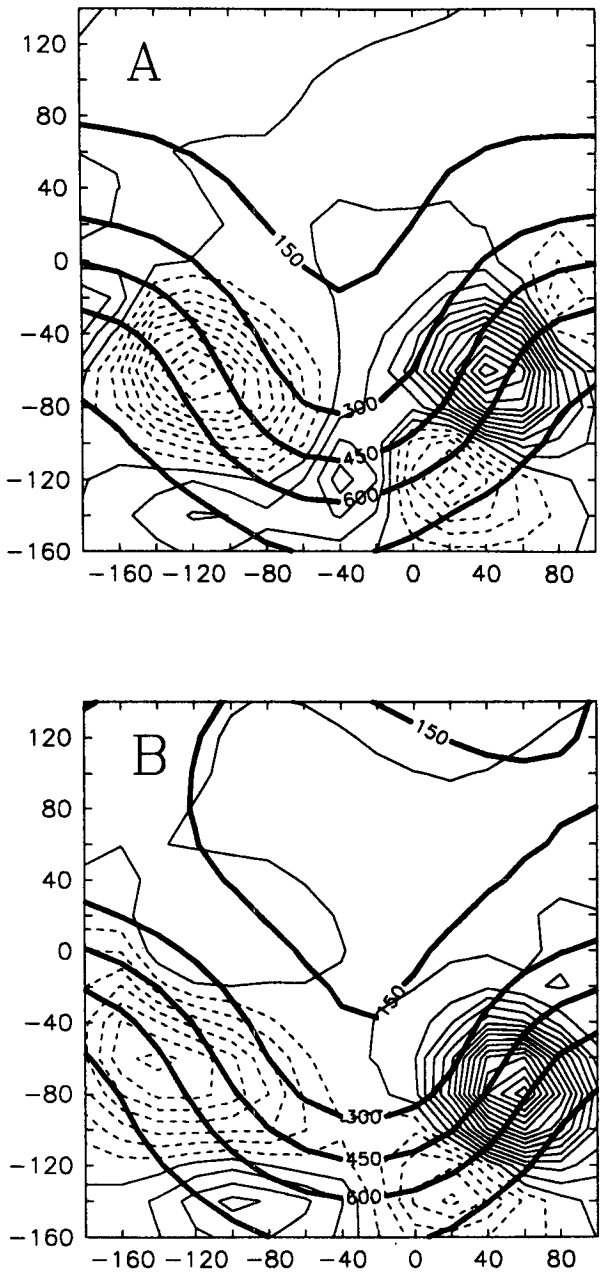

FIG. 11. Mapped thermocline topography—that is, z_{12}—(bold, contour interval 150 m) as measured by IES, overlain by w_{IES} computed from (4) (contour interval 0.25 mm s^{-1}, negative values dashed), (a) at 1200 UTC 19 May 1990 and (b) at 1200 UTC 27 May 1990. Note the stationarity of features. The maximum in downward vertical motion at (−120, −70) is also captured in the CM data for G3 (not shown).

as we observe, are consistent with atmospheric dynamics as described in Palmén and Newton (1969).

6. Summary and conclusions

We have computed and compared vertical motions from three different sources in the Gulf Stream downstream of Cape Hatteras. Magnitudes of vertical motion as measured by RAFOS floats and as estimated from CM data and IES data often reach values of 1–2 mm s^{-1} within the strong baroclinic front, with rare values of up to 3 mm s^{-1}. Both the CM and IES vertical motions are smoothly varying fields and are not dominated by the submesoscale and measurement noise that is present. It is easy to track features from day to day in both datasets; evolution of the fields occurs only slowly as mesoscale jet features evolve.

Current meter vertical motions agree closely with observations from RAFOS floats. There is also very good coherence at long timescales between w_{IES} and w_{CM} time series. Indeed, for timescales of greater than 16 days, w_{CM} and w_{IES} show coherence >0.5 at far above the 99% confidence level, but such coherence is absent for timescales of less than 12 d. The lack of coherence at short timescales is most likely associated with cases in which deep (barotropic) velocities are strong under the meandering Gulf Stream. By combining the IES data with an independent measure of the barotropic velocity, it should be possible to account for the vertical velocity driven by deep currents. It is also possible that there could be cases in which submesoscale features partially detected in CM data (and therefore evident in w_{CM}) are filtered out of the objectively mapped IES streamfunction fields (and therefore not present in w_{IES}); that is, submesoscale eddies could cause errors as shown in Panofsky (1951).

To our knowledge, this is the first study in which vertical motions associated with mesoscale processes in the ocean have been observed and verified by independent measurements and different dynamical diagnostic methods. The spatial and temporal structures of the w field can be diagnosed with both CM and IES arrays; the Gulf Stream clearly exhibits secondary circulations on the mesoscale that are consistent with quasigeostrophic dynamics.

Acknowledgments. We thank Meghan Cronin at URI for her considerable work in applying the mooring motion correction algorithm to the CM data. This study benefited greatly from fruitful discussions with Professor Tom Rossby (at URI) on RAFOS float technology, with Karen Tracey at URI on objective mapping of IES data, and with Dr. Melinda Hall at Woods Hole on current meter estimates of vertical motion, and from the perspicacious comments of two anonymous reviewers. Prof. John Young at the University of Wisconsin—Madison provided valuable comments on an earlier version of this work. This work was achieved with the support of the National Science Foundation (Grant OCE-8717144) and the Office of Naval Research (Contracts N00014-90J-1568 and N00014-92J-4013).

APPENDIX

Errors in Float Vertical Motion Estimates

Consider a pattern of vertical motion that along a fluid particle trajectory varies sinusoidally such that

the pressure measured by a RAFOS float and the vertical motion will be

$$P = A \sin\omega t$$

$$w_{\text{true}} \equiv \frac{\partial P}{\partial t} = -A\omega \cos\omega t, \qquad \text{(A1)}$$

respectively. How is the computed vertical motion affected by discrete, rather than continuous, sampling? The estimated vertical motion $\hat{w}$ from centered finite differencing is

$$\hat{w} = A \frac{\sin[\omega(t + \Delta t)] - \sin[\omega(t - \Delta t)]}{2\Delta t}$$

$$= w_{\text{true}} \frac{\sin\omega\Delta t}{\omega\Delta t}. \qquad \text{(A2)}$$

The ratio $\hat{w}/w_{\text{true}}$ approaches unity for all motions that have period $T(=2\pi/\omega)$ much longer than the sampling time Δt but it crosses zero for $T = 2\Delta t$.

The RAFOS floats that generated the data used in this study sampled data at $\Delta t = 8$ h. For $T \geq 3$ days, for example, $\hat{w}/w_{\text{true}} \geq 0.92$; however, for a period T of 36 h, the estimated vertical motion is 70% of true. Vertical motions in the inertial frequency range (or higher frequencies) are significantly underestimated by the 8-h sampling period. For a period of 19 h, for example, the estimated vertical motion is only 18% of the true. However, this is desirable, because we are using the floats to estimate vertical motions on meso- and synoptic scales.

The largest vertical motions that we investigate in this paper are typically associated with float displacements with a period 3 days or less. Several of the float trajectories through the central array show strong up and down couplets, with the float moving up and down >200 m in less than 3 days. Equation (A2) indicates that the vertical motion as measured by the float will underestimate the true vertical motion, perhaps by around 30% if the dominant period of the float is around 36 h.

REFERENCES

Anderson-Fontana, S., and H. T. Rossby, 1991: RAFOS floats in the SYNOP experiment 1988–1990. Tech. Rep. 91-7, University of Rhode Island Graduate School of Oceanography, Narragansett, RI, 155 pp.

Árnason, G., 1942: Distribution of mass variations in atmospheric air columns. *Meteor. Ann.*, **10,** 255–279.

Bane, J. M., L. M. O'Keefe, and D. R. Watts, 1989: Mesoscale eddies and submesoscale coherent vortices: Their existence near and interactions with the Gulf Stream. *Mesoscale/Synoptic Coherent Structures in Geophysical Turbulence,* J. C. J. Nihoul and B. M. Jamart, Eds., Elsevier, 501–518.

Blanton, S. L., III, 1991: Computations of vertical velocity in the Gulf Stream northeast of Cape Hatteras, North Carolina. M.S. thesis, University of North Carolina Marine Sciences Program, 84 pp.

Bower, A. S., 1989: Potential vorticity balances and horizontal divergence along particle trajectories in Gulf Stream meanders east of Cape Hatteras. *J. Phys. Oceanogr.*, **19,** 1669–1681.

——, 1991: A simple kinematic mechanism for mixing fluid parcels across a meandering jet. *J. Phys. Oceanogr.*, **21,** 173–180.

——, and H. T. Rossby, 1989: Evidence of cross-frontal exchange processes in the Gulf Stream based on isopycnal RAFOS float data. *J. Phys. Oceanogr.*, **19,** 1177–1190.

Bryden, H. L., 1976: Horizontal advection of temperature for low-frequency motions. *Deep-Sea Res.*, **23,** 1165–1174.

——, 1980: Geostrophic vorticity balance in midocean. *J. Geophys. Res.*, **85**(C), 2825–2828.

Fields, E., and D. R. Watts, 1990: THE SYNOP EXPERIMENT: Inverted Echo Sounder data report for May 1988 to Aug 1989. GSO Tech. Rep. 90-2, Graduate School of Oceanography, University of Rhode Island, Narragansett, RI, 231 pp.

——, and ——, 1991: THE SYNOP EXPERIMENT: Inverted Echo Sounder data report for Jun 1989 to Sep 1990. GSO Tech. Rep. 91-2, Graduate School of Oceanography, University of Rhode Island, Narragansett, RI, 255 pp.

Gill, A. E., 1982: *Atmosphere–Ocean Dynamics.* Academic Press, 662 pp.

Gilman, C. S., 1988: A study of the Gulf Stream downstream of Cape Hatteras 1975–1986. M. S. thesis, University of Rhode Island, 75 pp.

Hall, M. M., 1985: Horizontal and vertical structure of velocity, potential vorticity and energy in the Gulf Stream. Ph.D. thesis, Massachusetts Institute Of Technology/Woods Hole Oceanographic Institution Program, WHOI-85-16, Woods Hole, MA, 165 pp.

——, 1986: Horizontal and vertical structure of the Gulf Stream velocity field at 68°W. *J. Phys. Oceanogr.*, **16,** 1814–1828.

——, 1989: Energetics of the Kuroshio extension at 35°N, 152°E. *J. Phys. Oceanogr.*, **21,** 958–975.

Hogg, N. G., 1991: Mooring motion corrections revisited. *J. Atmos. Oceanic Technol.*, **8,** 289–295.

Holton, J. R., 1979: *An Introduction to Dynamic Meteorology.* Academic Press, 391 pp.

Kim, H.-S., and D. R. Watts, 1994: An observational streamfunction in the Gulf Stream. *J. Phys. Oceanogr.*, **24**(12), in press.

Leach, H., 1987: The diagnosis of synoptic-scale vertical motion in the seasonal thermocline. *Deep-Sea Res.*, **34,** 2005–2017.

Lee, T., 1993: Variability of the Gulf Stream path from Cape Hatteras to 45° west observed from infrared imagery. Ph.D. thesis, University of Rhode Island Graduate School of Oceanography, 95 pp.

Lindstrom, S. S., and D. R. Watts, 1993: Vertical Motion in the SYNOP Central Array. Tech. Rep. 93-2, University of Rhode Island Graduate School of Oceanography, Narragansett, RI, 84 pp.

Osgood, K. E., J. M. Bane Jr., and W. K. Dewar, 1987: Vertical velocities and dynamical balances in Gulf Stream meanders. *J. Geophys. Res.*, **92**(C), 13 029–13 040.

Palmén, E., and C. W. Newton, 1969: *Atmospheric Circulation Systems. Their Structure and Physical Interpretation.* Academic Press, 603 pp.

Panofsky, H. A., 1944: The effect of vertical motion on local temperature and pressure tendencies. *Bull. Amer. Meteor. Soc.*, **25,** 271–275.

——, 1951: Large-scale vertical velocity and divergence. *Compendium of Meteorology,* T. F. Malone, Ed., Amer. Meteor. Soc., 639–646.

Pickart, R. S., and D. R. Watts, 1990: Using the inverted echo sounder to measure vertical profiles of Gulf Stream temperature and geostrophic velocity. *J. Atmos. Oceanic Technol.*, **7,** 146–156.

Pollard, R. T., and L. A. Regier, 1992: Vorticity and vertical circulation at an ocean front. *J. Phys. Oceanogr.*, **22,** 609–625.

Rossby, H. T., 1987: On the energetics of the Gulf Stream at 73°W. *J. Mar. Res.*, **45,** 59–82.

——, D. Dorson, and J. Fontaine, 1986: The RAFOS system. *J. Atmos. Oceanic Technol.*, **3,** 672–679.

Shapiro, R., 1970: Smoothing, filtering and boundary effects. *Rev. Geophys. Space Phys.*, **8,** 359–387.

Shay, T. J., S. Haines, J. M. Bane, and D. R. Watts, 1994: SYNOP Central Array current meter data report: Mooring period May 1988–September 1990. University of North Carolina Tech. Rep. CMS 91–2, 106 pp.

Tintoré, J., D. Gomis, S. Alonso, and G. Parrilla, 1991: Mesoscale dynamics and vertical motion in the Alborán Sea. *J. Phys. Oceanogr.*, **21,** 811–823.

Tracey, K. L., and D. R. Watts, 1991: THE SYNOP EXPERIMENT: Thermocline depth maps for the Central Array October 1987 to August 1990. GSO Tech. Rep. No. 91-5, Graduate School of Oceanography, University of Rhode Island, Narragansett, RI, 193 pp.

Watts, D. R., 1983: Gulf Stream variability. *Eddies in Marine Science,* A. R. Robinson, Ed., Springer-Verlag, 114–144.

——, and H. T. Rossby, 1977: Measuring dynamic heights with inverted echo sounders: Results from MODE. *J. Phys. Oceanogr.*, **7,** 346–358.